AIP | The Journal of Chemical Physics

Restricted active space calculations of L-edge X-ray absorption spectra: From molecular orbitals to multiplet states

Rahul V. Pinjari, Mickaël G. Delcey, Meiyuan Guo, Michael Odelius, and Marcus Lundberg

Citation: The Journal of Chemical Physics **141**, 124116 (2014); doi: 10.1063/1.4896373
View online: http://dx.doi.org/10.1063/1.4896373
View Table of Contents: http://scitation.aip.org/content/aip/journal/jcp/141/12?ver=pdfcov
Published by the AIP Publishing

Restricted active space calculations of L-edge X-ray absorption spectra: From molecular orbitals to multiplet states

Rahul V. Pinjari,[1] Mickaël G. Delcey,[1] Meiyuan Guo,[1] Michael Odelius,[2] and Marcus Lundberg[1,a)]

[1]*Department of Chemistry - Ångström Laboratory, Uppsala University, SE-751 20 Uppsala, Sweden*
[2]*Department of Physics, Stockholm University, AlbaNova University Center, SE-106 91 Stockholm, Sweden*

(Received 9 June 2014; accepted 12 September 2014; published online 26 September 2014; corrected 30 September 2014)

The metal L-edge ($2p \rightarrow 3d$) X-ray absorption spectra are affected by a number of different interactions: electron-electron repulsion, spin-orbit coupling, and charge transfer between metal and ligands, which makes the simulation of spectra challenging. The core restricted active space (RAS) method is an accurate and flexible approach that can be used to calculate X-ray spectra of a wide range of medium-sized systems without any symmetry constraints. Here, the applicability of the method is tested in detail by simulating three ferric ($3d^5$) model systems with well-known electronic structure, viz., atomic Fe^{3+}, high-spin $[FeCl_6]^{3-}$ with ligand donor bonding, and low-spin $[Fe(CN)_6]^{3-}$ that also has metal backbonding. For these systems, the performance of the core RAS method, which does not require any system-dependent parameters, is comparable to that of the commonly used semi-empirical charge-transfer multiplet model. It handles orbitally degenerate ground states, accurately describes metal-ligand interactions, and includes both single and multiple excitations. The results are sensitive to the choice of orbitals in the active space and this sensitivity can be used to assign spectral features. A method has also been developed to analyze the calculated X-ray spectra using a chemically intuitive molecular orbital picture. © *2014 AIP Publishing LLC*. [http://dx.doi.org/10.1063/1.4896373]

I. INTRODUCTION

First-row transition metals are key components in many homogeneous and heterogeneous catalysts. For these systems, metal L-edge (2p → 3d) X-ray absorption spectroscopy (XAS) offers an element-specific probe, which directly targets the unoccupied or partially unoccupied 3d orbitals acting as electron acceptors during catalytic reactions. To get the most out of the L-edge XAS data, a theoretical method is required that can relate the spectral shape to the electronic structure of the system. Due to the complexity of the $(2p)^5(3d)^{n+1}$ final states, such a method must be able to accurately describe a large number of different effects: 2p-3d and 3d-3d electron-electron repulsion, as well as 2p and 3d spin-orbit coupling (SOC).

Several methods have been designed to model L-edge XAS spectra, e.g., the Bethe-Salpeter equation,[1,2] the multichannel multiple scattering method,[3,4] and several different approaches based on configuration interaction (CI) calculations.[5–14] The major differences between the CI-based methods are the description of electron correlation, the selection of electronic configurations, and the treatment of spin-orbit coupling.

A widely used and computationally efficient method is the semi-empirical ligand-field multiplet (LFM) model.[5] In this atomic model, initial and final states are calculated from a full CI including the 3d orbitals. This treatment takes into account all possible 3d electron configurations. Electron correlation is introduced by reducing the electron-electron repulsion integrals from their Hartree-Fock values. Spin-orbit coupling is included in the Hamiltonian at the same level as electron-electron repulsion. Ligands are described by an empirical ligand-field splitting of the 3d orbitals.

For highly covalent complexes, the effects of ligands can be modeled using additional configurations, where one electron has been transferred from or to the ligand, i.e., ligand-to-metal charge transfer (LMCT) or metal-to-ligand charge transfer (MLCT) configurations. Adding these configurations to the CI gives the semi-empirical charge-transfer multiplet (CTM) model.[6,7] This method gives a balanced description of electron-electron repulsion and spin-orbit coupling and includes all relevant final states. The amount of metal-ligand mixing is typically determined from a system-dependent multi-parameter fit to the experimental spectrum. The number of model parameters increases with decreasing symmetry, and the semi-empirical CTM approach thus works best for complexes with a high degree of symmetry.

Ab initio methods offer better predictive power than semi-empirical ones, at least in principle. In the *ab initio* LFM model, the basis for the CI calculations are molecular orbitals (MOs) calculated for small clusters, typically the central atom and first-shell ligands. The SOC is introduced at the MO level through a relativistic four-component calculation (j-j coupling), while electron correlation is introduced by calculating the MOs using density-functional theory (DFT). To minimize the computational cost, the CI calculations are performed using a limited number of determinants, e.g., those corresponding to single excitations from 2p to 3d, as well as

a)Electronic mail: marcus.lundberg@kemi.uu.se

within the 3d space.[8,15] In the *ab initio* LFM model, the effects of the ligands are accounted for in the calculations of the molecular orbitals. An extension to the method is to include ligand-centered orbitals also in the CI, giving the *ab initio* CTM model. To limit the number of new configurations, only single excitations from the ligand orbitals are typically included in the expansion.[9,16]

A drawback of the *ab initio* CTM model is that it can only be applied to relatively small clusters. To overcome this limitation, one can perform a plane-wave local-density approximation (LDA) DFT calculation and get localized metal 3d and ligand orbitals using Wannier functions.[10] These functions can then be used to calculate most of the parameters in a CTM model, but the spherical part of the 2p-3d and 3d-3d Coulomb correlation and the charge-transfer energy must still be fitted to experimental data.

The DFT restricted-open shell configuration interaction with singles (DFT/ROCIS) approach has been developed for clusters up to 30 metal atoms.[11,12,17] In this method, the CI is performed on the non-relativistic orbitals and includes only single excitations, i.e., the core to valence excitation. To cover all the multiplets arising from the atomic terms, relevant spin multiplicities are calculated and the magnetic sublevels are constructed using Wigner-Eckart algebra. The description of electron correlation is improved by parameterizing the configuration interaction matrix, using three system-independent parameters. Finally, SOC is included through a quasi-degenerate perturbation approach on the non-relativistic states, which is the molecular equivalent of atomic L-S coupling.

Allowing only single excitations in the CI expansion ignores the higher-order excitations and limits the description of the X-ray process.[13] In the complete active space (CAS) self-consistent field (SCF) method, a full CI is constructed among the active orbitals.[18,19] This multiconfigurational wavefunction method has been widely used to model valence excitations, but can be adapted for X-ray processes by including also the core orbitals in the active space. As the number of excitations from the core orbitals can be restricted, usually to one, it is convenient to use the restricted active space SCF (RASSCF) method,[20] giving the core RAS method.

The valence active space in the RASSCF approach can either include only the metal-centered 3d MOs, giving a ligand-field model, or also the important ligand MOs, giving a charge-transfer model. Unlike the other *ab initio* methods, the full CI calculation in the active space not only spans the correct final states, but also accounts for the correlation between active electrons. The calculation can further be improved by including correlation with the occupied inactive and virtual orbitals using second order perturbation (RASPT2).[21–23] SOC is added on top of the multiconfigurational spin-free states, which is equivalent to L-S coupling.

The core RAS method can be applied to similar systems that are currently treated using standard RASPT2, i.e., systems with ∼50 atoms even without any symmetry. It has already been applied to the X-ray photoelectron spectra (XPS) of U and Yb compounds,[24] and I_3^-,[25] as well as L-edge XAS spectra of transition-metal coordination complexes.[14,26–29] The ability of RASSCF to treat near-degenerate electronic states makes it appropriate for investigations with time-resolved X-ray spectroscopy since the photo-excited compounds that undergo changes in chemical bonding can also be studied.[25] The recent development of sources for time-resolved resonant inelastic X-ray scattering (RIXS) techniques enables insight into both ultra-fast electron dynamics and nuclear dynamics. The RASSCF framework is suitable for a detailed description of dynamical and polarization dependence in the RIXS and X-ray emission processes and has been applied to calculate the RIXS spectra of aqueous Ni^{2+},[14,30] as well as ferrocyanide and ferrocene.[29]

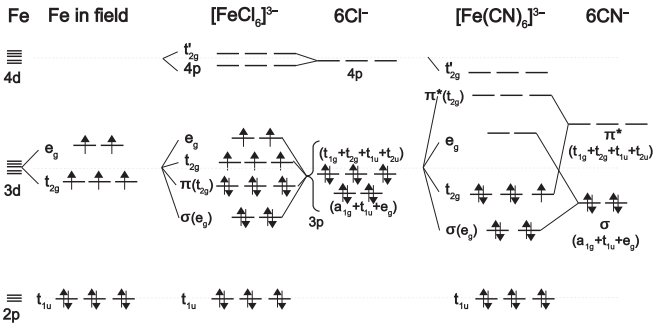

FIG. 1. Schematic molecular orbital diagrams for high-spin ($^6A_{1g}$) Fe^{3+} and $[FeCl_6]^{3-}$, as well as low-spin ($^2T_{2g}$) $[Fe(CN)_6]^{3-}$.

Although core RAS is an *ab initio* method, its accuracy and computational cost can be tuned through the design of the active space and the choice of excitation levels in the valence space. This flexibility necessitates an understanding of how these choices affect the performance, but this has not yet been properly established. In the present study, the performance of the core RAS method is therefore tested by applying it to a series of L-edge XAS spectra of ferric ($3d^5$) reference systems with well-known electronic structures. In O_h symmetry, the high-spin $3d^5$ systems have $(t_{2g})^3(e_g)^2$ configurations and $^6A_{1g}$ ground states, which give the maximum number of unpaired 3d electrons in any system. The low-spin $3d^5$ systems have $(t_{2g})^5$ configurations and orbitally degenerate $^2T_{2g}$ ground state, a difficult case for many theoretical models.

The first test case, the Fe^{3+} atomic ion in different crystal fields, enables a one-to-one comparison with the semi-empirical LFM model. The second case, $[FeCl_6]^{3-}$ (ferric chloride), is a high-spin system with prototypical σ and π-donor ligands, see Fig. 1. This system corresponds to a CTM model with an extra LMCT configuration. The third case, $[Fe(CN)_6]^{3-}$ (ferricyanide), is a low-spin complex where the empty π^* CN^- ligands gives rise to π-backdonation, see Fig. 1. In the CTM model, this corresponds to a three-configuration calculation with an additional MLCT configuration. These systems can be used to establish the performance of the core RAS method for a variety of bonding situations, which will open up for applications in more complex systems.

One of the advantages of a molecular orbital approach is the possibility to analyze the electronic structure in a chemically intuitive way. However, this intuition is often lost in large CI calculations. A method will therefore be developed that can interpret the complicated multiplet spectra in terms of excitations to, and from, different molecular orbitals. This

analysis can be used to relate differences in L-edge XAS spectra to the electronic structure, which would add significant value to the theoretical analysis.

II. COMPUTATIONAL DETAILS

A. Core RAS method

The RASSCF/RASPT2 calculations have been performed with MOLCAS 7.9.[31] The active space is labeled RAS (*n,l,m;i,j,k*), where, *i,j* and *k* are the number of orbitals in the RAS1, RAS2, and RAS3 spaces, respectively, *n* is the total number of electrons in the active space, *l* the maximum number of holes allowed in RAS1, and *m* the maximum number of electrons in RAS3. The minimum valence active space consists of the metal-dominated 3d orbitals. The first additions to this space should be orbitals that correlate strongly with them, i.e., the bonding or antibonding partners. For filled or partly filled d shells, an additional empty shell with the same symmetry and metal 4d character can be included for correlation, the double-shell effect.[32] The 2p orbitals have been placed in the RAS1 space, allowing a maximum of one hole.

RASSCF optimizations have been performed using the state average (SA) formalism, which means that the same orbitals are used for all the final states of a specific spin and symmetry. A relatively large level shift of 1.0 hartree (h) has been applied to achieve convergence for all different RAS spaces. To avoid orbital rotation, i.e., to ensure that the core excitation occurs from the 2p instead of the higher-lying 3p orbitals, the former have been frozen in the RASSCF optimizations. Relaxing the 2p orbitals would lower the energies of all the excited states, which would mainly affect the energy shift required to overlay calculated and experimental spectra.

RASPT2 calculations have been performed using multistate (MS) RASPT2.[33] For valence excitations, the default RASPT2 procedure is that the core orbitals, 1s of C/N and up to 3s of Cl/Fe, are frozen. Calculations where the core orbitals have been correlated are labeled RASPT2-cc. The RASPT2 and RASPT2-cc calculations have been performed using the default ionization potential electron affinity (IPEA) shift of 0.25 hartree,[34] and an imaginary shift of 0.3 hartree to reduce problems with intruder states.[35]

Scalar relativistic effects have been included through a Douglas-Kroll (DK) Hamiltonian[36,37] in combination with a relativistic atomic natural orbital (ANO-RCC) basis set.[38,39] Unless specified, a basis set of triple-ζ quality (ANO-RCC-VTZP) has been used. To speed up calculations without sacrificing accuracy, the density-fitting approximation of the electron-electron repulsion integrals has been used, employing auxiliary basis sets from an atomic-compact Cholesky decomposition.[40–42]

Spin-orbit coupling is included from a one-electron spin-orbit Hamiltonian based on atomic mean field integrals.[43] The spin-free eigenstates are used as a basis for computing spin-orbit interaction matrix elements, and the spin-orbit eigenstates are then obtained by diagonalizing the spin-orbit interaction matrix,[44] giving SOC states ($|\Lambda\rangle$), which are linear combinations of spin-free states ($|I\rangle$):

$$|\Lambda\rangle = \sum_I c_I^{\Lambda} |I\rangle. \tag{1}$$

These eigenstates are then utilized to calculate the strength of the electric dipole transitions using the restricted active space state interaction (RASSI) approach.[45,46] The intensity of a transition is proportional to the square of the expectation value of the dipole operator:

$$\langle \Lambda|\hat{d}|\Theta\rangle^2 = \left(\sum_I c_I^{\Lambda} \sum_J c_J^{\Theta} \langle I|\hat{d}|J\rangle\right)^2. \tag{2}$$

An example of the coupling scheme, from RASSCF spin-free states to SOC states is given in Fig. 2.

Although the model systems have O_h or D_{4h} symmetry, calculations are effectively performed in D_{2h}, which is the highest symmetry Abelian point group. This point group has inversion symmetry, and out of the active orbitals only the 2p orbitals are of ungerade symmetry. All states of ungerade symmetry are thus core excited states. In the RASSCF calculations of the final state, all four irreducible representations with ungerade symmetry in D_{2h} (A_{1u}, B_{1u}, B_{2u}, and B_{3u}) have been included. The calculations also include all possible $(2p)^5(3d)^6$ spin states: doublet, quartet, and sextet. For the atomic calculations, where only the five 3d orbitals are placed in the active space, all final states are included in the

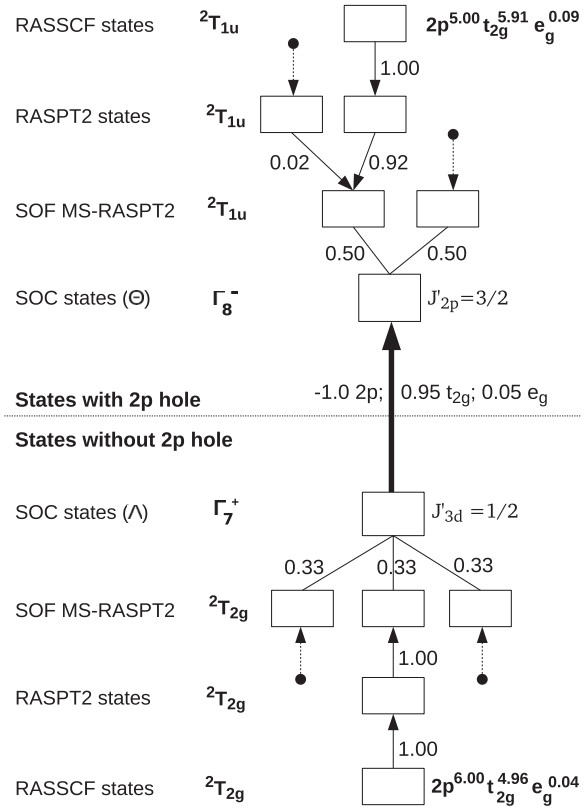

FIG. 2. Coupling scheme between states and molecular orbitals for the $2p \rightarrow t_{2g}$ peak in the L_3-edge of the low-spin Fe^{3+} ion. The weights of the states are shown next to the thin arrows. Only selected states are displayed and equivalent states are shown as dots. The thick arrow represents the core excitation and the numbers next to the arrow show the changes in occupation numbers of the molecular orbitals.

calculations. For B_{1u}, B_{2u}, and B_{3u}, this means 72 doublet, 37 quartet, and 4 sextet states each, while the corresponding numbers for A_{1u} symmetry are 69, 39, and 0. Including also ligand orbitals in the active space gives a very large number of possible final states. For these systems, calculations have been performed with a fixed number of final states per symmetry and spin multiplicity. Up to 120 states have been calculated for all the 12 symmetry-spin combinations, which gives a total of 1440 final states before spin-orbit coupling. The final spectrum is sensitive to the number of states but with 120 states the shapes of the L_3 edges appear to be converged.

B. Analysis of orbital contributions

In the core RAS approach, the L-edge XAS spectrum can be analyzed in terms of chemically intuitive molecular orbitals and their occupation numbers. Natural occupation numbers for the active orbitals are available for each RASSCF state, and can be constructed for MS-RASPT2 and RASSI SOC states as they are just linear combinations of RASSCF states, see Fig. 2. The differences in occupation numbers between the ground state and each final state allows for an intuitive interpretation of the spectrum in terms of orbital excitations. However, the spin-free states mix heavily under the influence of the strong spin-orbit coupling in the final state. This complicates a straightforward analysis. Instead, an approximate scheme was designed in which only the spin-free states contributing to the final intensity of a transition between SOC states were taken into account. Assuming that the effect of the cross-terms in Eq. (2) are similar for the different spin-free contributions and therefore can be neglected, this gives:

$$\langle \Lambda \mid \hat{d} \mid \Theta \rangle^2 \approx \sum_I \omega_I^\Lambda \sum_J \omega_J^\Theta \langle I \mid \hat{d} \mid J \rangle^2 \qquad (3)$$

with the weights $\omega_I^\Lambda = (c_I^\Lambda)^2$. This summation uses only information printed in the MOLCAS output, although the code has been modified to include all contributions with weights $>10^{-5}$. The change in natural occupation number between the spin-free states is then weighted by the estimate in Eq. (2). Using n_I^i for the natural occupation number of orbital i in the spin-free state I and $f(I \rightarrow J)$, the intensity of the transition between spin-free states I and J, the contribution of orbital i to the intensity of a transition from the initial state Λ to the final state Θ, $f_i(\Lambda \rightarrow \Theta)$, was computed as

$$f_i(\Lambda \rightarrow \Theta) = \frac{\sum_I \omega_I^\Lambda \sum_J \omega_J^\Theta f(I \rightarrow J)\left(n_J^i - n_I^i\right)}{\sum_I \omega_I^\Lambda \sum_J \omega_J^\Theta f(I \rightarrow J)} f(\Lambda \rightarrow \Theta). \qquad (4)$$

Because of the large number of transitions, an analysis for each individual transition is not desirable and a graphical representation that adds all contributions is used instead.

C. Core RAS model systems

To simulate a ligand-field splitting in the atomic system, six negative charges are placed at the vertices of the octahedron, 2.0 Å away from the Fe^{3+} center. This is an arbitrary distance representing a typical metal-ligand distance. Using this distance, charges more negative than −8.0 a.u. creates a strong field as they lead to a stable low-spin $^2T_{2g}$ state. Simulations have been performed with zero charges, −5.3 a.u. (weak field) and −12.4 a.u. (strong field). The last two sets of charges give the same energy difference between the lowest spin states as in the RASPT2 calculations of ferric chloride ($^6A_{1g}$ 2.20 eV below $^2T_{2g}$) and ferricyanide ($^2T_{2g}$ 2.61 eV below $^4T_{1g}$). The model charges have to be unphysically large to get the correct spin-state energetics in the crystal field model because in molecular systems the ligand-field splitting is mainly caused by the mixing of metal and ligand orbitals.

All spectral simulations of molecular systems have been performed using the ground state geometries. Calculations on $[FeCl_6]^{3-}$ have been performed on an O_h-symmetric structure with Fe-Cl distances of 2.40 Å, which is between 2.39 and 2.41 Å as revealed from X-ray diffraction studies.[47–50] The $[Fe(CN)_6]^{3-}$ geometry is optimized at the CASPT2/ANO-RCC-VTZP (9,0,0;0,10,0) level, giving four Fe-C distances of 1.939 Å and two distances of 1.916 Å, in good agreement with experimental estimates of 1.941 Å.[51] The C-N distances are 1.178 (1.180) Å. Ferricyanide thus has D_{4h} symmetry, but, as will be shown below, the effects of this distortion are relatively small and O_h symmetry will be used in the interpretation of the results.

D. Semi-empirical CTM model

Calculations with the semi-empirical CTM model have been performed using the program TT-Multiplets.[52] The model includes an atomic description of electron-electron interactions and spin-orbit coupling with the ligand-field splittings introduced as parameters.[5] Electron-electron repulsion integrals, calculated at the Hartree-Fock (HF) level, are scaled by 80% to mimic electron correlation. Atomic systems are calculated without field, and with ligand fields (10Dq) of 2.175 eV (weak field) and 4.984 eV (strong field) that reproduce the ^6A_g - $^2T_{2g}$ and $^2T_{2g}$ - $^4T_{1g}$ splittings in the simulations of $[FeCl_6]^{3-}$ and $[Fe(CN)_6]^{3-}$. The simulations of $[FeCl_6]^{3-}$ are made with a main atomic configuration (d^n) and a LMCT configuration ($d^{n+1}\underline{L}$)) that describes σ and π-donation. Here $\underline{L}$ symbolizes a ligand hole. The amount of mixing is determined by the charge-transfer energy between main and LMCT configurations (Δ) and the covalent mixing terms (T_α) for each irreducible representation of the 3d orbitals. These parameters are taken from reference Wasinger *et al.*[53] The $[Fe(CN)_6]^{3-}$ spectrum has been simulated with an additional MLCT configuration using the parameters from Hocking *et al.*[51] The list of parameters for all multiplet simulations are given in Table 1 in the supplementary material.[54]

E. Experimental comparisons

The experimental spectra of ferric chloride and ferricyanide are taken from Wasinger *et al.*[53] and Hocking *et al.*[51] To obtain L-edge XAS spectra from the core RAS and VBCI multiplet models, the transition intensities are plotted using a Lorentzian broadening with a full-width-at-half-maximum

(FWHM) of 0.4 and 0.8 eV for the L_3 and L_2 edge.[55,56] The spectra are further convoluted with an experimental Gaussian broadening of 0.4 eV. With this broadening, the FWHM of the first major transition in the ferricyanide is similar in simulated and experimental spectra.[51]

For $[FeCl_6]^{3-}$, the energy scales of calculated and experimental spectra are aligned at the most intense peak (∼708 eV). This gives a shift of −2.68 eV for the RASPT2-cc(15,1,0;3,10,0)/ANO-RCC-VTZP simulation. For $[Fe(CN)_6]^{3-}$, the spectra are aligned at the first intense transition (∼706 eV), which gives a shift of −2.93 eV for the RASPT2-cc(15,1,0;3,10,0)/ANO-RCC-VTZP simulation.

III. RESULTS

A. Atomic systems

Results are presented in order of increasing complexity of the electronic structure, starting with the monoatomic Fe^{3+} system having six point charges in O_h symmetry. The RAS1 space includes the three 2p orbitals (t_{1u}) while the RAS2 space includes the five 3d orbitals (t_{2g} and e_g), see Fig. 1. This gives a total of 11 active electrons. With one excitation allowed from the RAS1 space, and no orbitals in the RAS3 space, the active space is written as RAS(11,1,0;3,5,0). In all atomic calculations, the ANO-RCC...3s2p1d basis set contraction has been used.

The L-edge XAS spectra of the Fe^{3+} ion calculated using the core RAS and semi-empirical LFM models without external field, with a weak field, and with a strong field, are displayed in Fig. 3. For the systems with a high-spin $^6A_{1g}$ $(t_{2g})^3(e_g)^2$ ground state, the core RAS and multiplet spectra agree very well up to 717 eV in the L_3 edge. Above this energy, the core RAS spectra has a minor peak, absent in the multiplet calculations, see Figs. 3(a) and 3(b). The shape of the L_2-edge region above 720 eV is also different. However, the L-edge spectra of the low-spin $^2T_{2g}$ $(t_{2g})^5(e_g)^0$ system calculated with the core RAS and multiplet model match over the entire energy region. One of the minor differences is that the L_2 edge appears at lower energies in the core RAS spectrum.

To understand the core RAS results, the spectrum from the low-spin $^2T_{2g}$ ground state is analyzed in more detail, starting with the effects of 2p and 3d SOC, see Fig. 4. As expected, without any SOC there is a single edge, split by ligand-field and multiplet effects. Proper inclusion of 2p spin-orbit coupling, dashed line in Fig. 4, not only splits the spectrum into L_3 ($J'_{2p} = \frac{3}{2}$) and L_2 ($J'_{2p} = \frac{1}{2}$) edges, but also leads to major changes in spectral shape because of the mixing of states with different multiplicity. To form the correct spin-orbit states requires all three 2p orbitals, and the size of the core RAS1 space can therefore not be decreased. Due to mixing caused by the 2p-3d multiplet interactions, the final states are not pure $J_{2p} = \frac{3}{2}$ and $J_{2p} = \frac{1}{2}$ states, and J' has therefore been used as a convenient label.

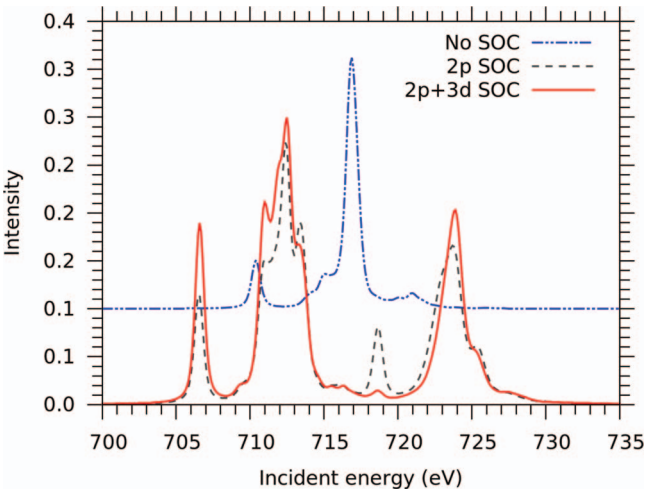

FIG. 4. Core RAS L-edge XAS spectra of the low spin Fe^{3+} ion with different treatments of 2p and 3d SOC; without SOC (dashed-dotted line), with 2p SOC but using one of the $^2T_{2g}$ ground states, i.e., without considering splitting from 3d SOC (dashed line), and including both 2p and 3d SOC with a Boltzmann distribution of Γ_7^+ ($J'_{3d}=\frac{1}{2}$) and Γ_8^+ ($J'_{3d}=\frac{3}{2}$) initial states (solid line).

The spin-orbit coupling constant for the 3d orbitals is ≈0.05 eV, which is much weaker than ≈8 eV for the 2p orbitals. Despite the relatively small effect on the final-state energies, accounting for 3d SOC leads to visible changes in the calculated spectrum, especially in the intensities of both the $2p \rightarrow t_{2g}$ peaks, see Fig. 4. As the final state with $(2p)^5(t_{2g})^6(e_g)^0$ configuration is not affected by 3d SOC, the explanation must come from the $^2T_{2g}$ $(2p)^6(t_{2g})^5(e_g)^0$ ground state. Without spin-orbit coupling, the ground state is six-fold degenerate due to a three-fold orbital degeneracy and a doublet spin multiplicity. The SOC split these six states into doubly-degenerate $J'_{3d}=\frac{1}{2}$, Γ_7^+ in Bethe double-group

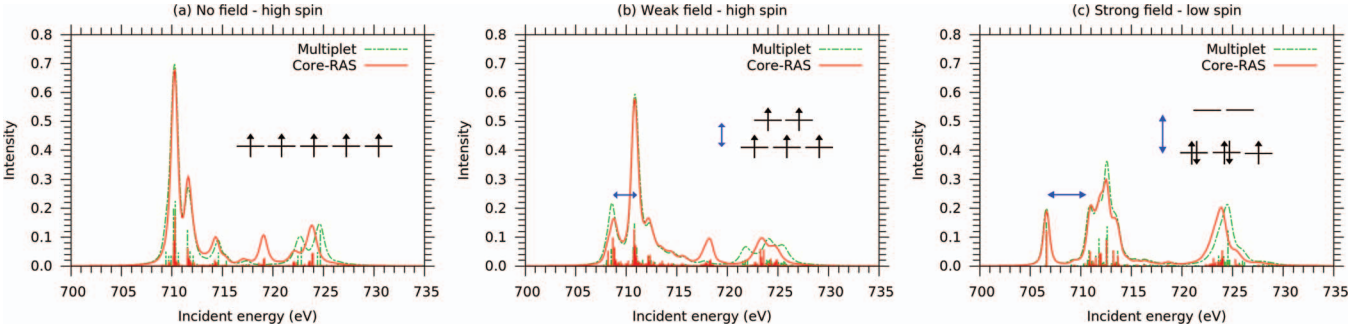

FIG. 3. L-edge XAS spectra of the Fe^{3+} ion, with different ligand-field splitting, calculated using RASPT2(11,1,0;3,5,0) (red solid line) and the ligand-field multiplet model (green dotted line). The lengths of the arrows give the approximate sizes of the ligand-field splittings.

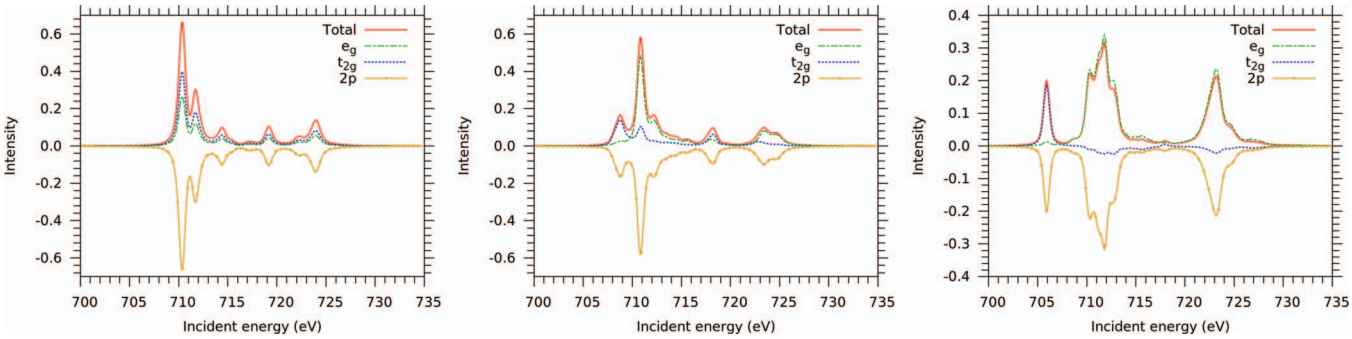

FIG. 5. Analysis of orbital contributions to the RASPT2(11,1,0:3,5,0) L-edge XAS spectra of the Fe^{3+} ion.

notation, and four-fold degenerate Γ_8^+ ($J'_{3d} = \frac{3}{2}$) states, with the Γ_7^+ states 0.086 eV lower in energy, see Fig. 1 of the supplementary material.[54] The changes in spectral shape are due to differences in selection rules for the different SOC states. As an example, transitions to the L_2 t_{2g} peak (Γ_6^-) are electric dipole forbidden from a Γ_7^+ ground state.[51] The weak L_2 t_{2g} intensity that can still be seen, comes from the Boltzmann population of Γ_8^+ states at room temperature (3.5%), see Fig. 2 of the supplementary material.[54] The 3d SOC also leads to changes in the broad $2p \rightarrow e_g$ resonance, partly not only due to the transitions to the Γ_6^- states get weaker, but also due to other differences in the intensity mechanisms that come from the change in the ground state.[57]

The previous analysis illustrates how the L-edge XAS spectrum is formed by the interactions between different electronic states. Despite this complexity, the spectral shape can be analyzed using an intuitive picture of molecular orbital excitations. The first peak in the L_3 edge of the low-spin Fe^{3+} ion, see Fig. 3(c), serves as a simple example. The Γ_7^+ ground state is formed from the three degenerate T_{2g} spin-free MS-RASPT2 states with equal ($\frac{1}{3}$) weights, see Fig. 2. Each MS-RASPT2 state is formed from a single dominant RASSCF state, where each RASSCF state represents a different position of an unpaired electron in the three t_{2g} (d_{xy}, d_{xz}, d_{yz}) orbitals. The full CI between the 3d orbitals in the RASSCF calculation gives occupation numbers of 4.96 and 0.04 for the t_{2g} and e_g orbitals, respectively, compared to 5.0 and 0.0 for an SCF calculation. The deviation from integer values is due to the use of excited determinants to describe correlation in wavefunction theory, which is different from the physical excitation process connected to the absorption of a photon.

The $2p \rightarrow t_{2g}$ excitation in the L_3 edge, caused by absorption of an X-ray photon, gives quadruply degenerate Γ_8^- ($J'_{2p} = \frac{3}{2}$) final states. They are formed by linear combinations of the T_{1u} spin-free MS-RASPT2 states, each of which has a dominant contribution (92%) from a single RASSCF state with occupation numbers of 5.91 for t_{2g} and 0.09 for e_g. Thus, the final state has a stronger t_{2g}-e_g correlation compared to the ground state. Weighing the contributions from all different configurations, the formal $2p \rightarrow t_{2g}$ excitation leads to the loss of one 2p electron, and a gain of 0.95 t_{2g} and 0.05 e_g electrons.

A graphical analysis of the orbital contributions to all final state excitations, as described in Sec. II B, is shown in Fig. 5. For the atomic systems, which only have t_{2g} and e_g orbitals in the valence active space, the analysis is straightforward. Without any field, e_g and t_{2g} orbitals are equivalent and the relative contributions simply reflect the different number of holes in the ground state. For the high-spin system (weak field), the first peak is mainly a $2p \rightarrow t_{2g}$ excitation, while the second resonance is a mixture of different multiplets reached by both $2p \rightarrow t_{2g}$ and $2p \rightarrow e_g$ transitions, where excitations to e_g orbitals dominate at higher incident energies. The low-spin system has a clear separation of t_{2g} and e_g resonances, and the small negative t_{2g} contributions in the e_g resonance reflect differences in correlation between initial and final state.

B. Ferric chloride $[FeCl_6]^{3-}$

Ferric chloride is a complex with prototypical σ and π-donor bonding. In O_h symmetry, the eighteen filled 3p Cl^- orbitals form six σ symmetry adapted linear combinations (SALCs) and twelve π SALCs. The two σ SALCs of e_g symmetry mix with metal 3d e_g orbitals to create bonding (σ) and antibonding (σ^*) combinations, see Fig. 1. The bonding orbitals have predominantly ligand character, while the σ^* orbitals are usually referred to as metal 3d e_g orbitals. The three filled π SALCs of t_{2g} symmetry mix with the 3d t_{2g} orbitals to form sets of relatively weakly bonding and antibonding molecular orbitals.

The ground state of ferric chloride is the high-spin $^6A_{1g}$ state with a formal $(t_{2g})^3(e_g)^2$ electron configuration. The RAS1 space consists of the three t_{1u} (Fe 2p) orbitals. The design of the RAS2 space starts with the metal-dominated three t_{2g} orbitals and two e_g orbitals. As the e_g orbitals participate in strong covalent interactions, the first extension is to include correlating orbitals in the same bond, i.e., the two ligand-dominated σ orbitals. The half-filled metal t_{2g} orbitals can either correlate with their bonding partners, the filled ligand-dominated t_{2g} (π) orbitals, or a set of empty 4d t_{2g} orbitals (t'_{2g}). In the ground state RASSCF calculation, the correlation is stronger with the t'_{2g} orbitals and they are therefore included in the active space, giving a total of ten RAS2 orbitals, see Fig. 3 of the supplementary material.[54]

As the RASSCF calculations are performed using the state-average approach, the orbital optimization depends on the states included therein. In final state calculations, the optimal orbitals may therefore be different from those in the

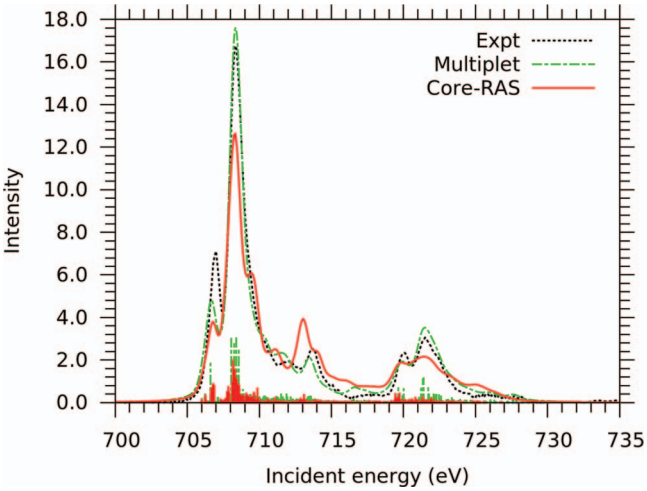

FIG. 6. L-edge XAS spectra of $[FeCl_6]^{3-}$ from RASPT2-cc(15,1,0;3,10,0)/ANO-RCC-VTZP with 120 states (red solid line), from the semi-empirical charge-transfer multiplet model (green dashed-dotted line), and from experiment (black dotted line).[53]

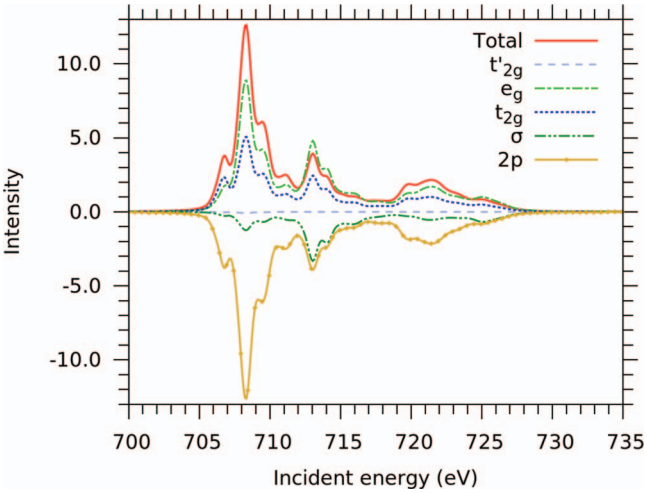

FIG. 7. Orbital analysis for the $[FeCl_6]^{3-}$ L-edge XAS spectrum calculated with RASPT2-cc/ANO-RCC-VTZP (15,1,0:3,10,0) and 120 states per symmetry and spin state.

ground state. For $[FeCl_6]^{3-}$, the lowest-lying unoccupied orbitals of t_{2g} symmetry are SALCs from the Cl 4p orbitals and in some calculations with a large number of states the metal 4d (t'_{2g}) orbitals are rotated out of the active space and replaced by the empty Cl 4p (t_{2g}) orbitals, see Fig. 3 of the supplementary material.[54] What appears to be large changes in the active-space orbitals caused by the core hole potential can instead be a consequence of orbital rotation in the RASSCF optimization. This orbital rotation does not compromise the applicability of the RASSCF method, as long as the energies are accurately calculated; however, it may complicate the analysis of the X-ray process.

The L-edge XAS spectrum calculated at the RASPT2-cc(15,1,0;3,10,0)/ANO-RCC-VTZP level with 120 states per final state symmetry and spin state is shown in Fig. 6. The core RAS spectrum predicts all the major and minor peaks of $[FeCl_6]^{3-}$, albeit the intensities of the first two peaks are underestimated. A peak at 714 eV in the experimental spectrum appears at 713.2 eV with too high intensity. The semi-empirical CTM model gives a slightly better estimate of the experimental shape; however, the core RAS results must be considered very good as they are obtained without fitting any parameter. The core RAS results are also significantly better than those previously obtained by the DFT/ROCIS method.[11]

The X-ray spectrum of $[FeCl_6]^{3-}$ can be analyzed using the approach employed for the atomic systems, see Fig. 7. The first band at 707 eV is mainly a $2p \rightarrow t_{2g}$ transition, while transitions in the main peak are mixtures of multiplets formed from t_{2g} and e_g excitations. The negative contribution from the σ orbitals highlights differences in correlation between metal and ligand orbitals in the final states compared to the ground state. These differences emphasize the importance of including the ligand-dominated orbitals in the active space. In comparison, the contributions from the metal t'_{2g} orbitals are almost negligible.

The insight provided by the orbital picture is even clearer in the analysis of the peak at 713.2 eV. Here the contributions from the ligand σ orbitals correspond to the loss of approximately one electron. The peak can therefore directly be assigned to a 2p excitation combined with a $\sigma \rightarrow 3d$ transition, i.e., a shake-up transition of LMCT type. This assignment is in agreement with a previous analysis using the semi-empirical CTM model.[53]

Although the core RASPT2-cc (15,1,0;3,10,0)/ANO-RCC-VTZP calculations show very good results, they are much more expensive than those of the DFT/ROCIS method. It is therefore interesting to see whether the computational cost can be decreased without any significant loss in accuracy. An obvious solution is to decrease the size of the active space. Figure 8 shows the minor differences between the original (15,1,0;3,10,0) active space and a (15,1,0;3,7,0) space where the empty orbitals of t_{2g} symmetry have been removed from the active space. The effect is only noticeable in the

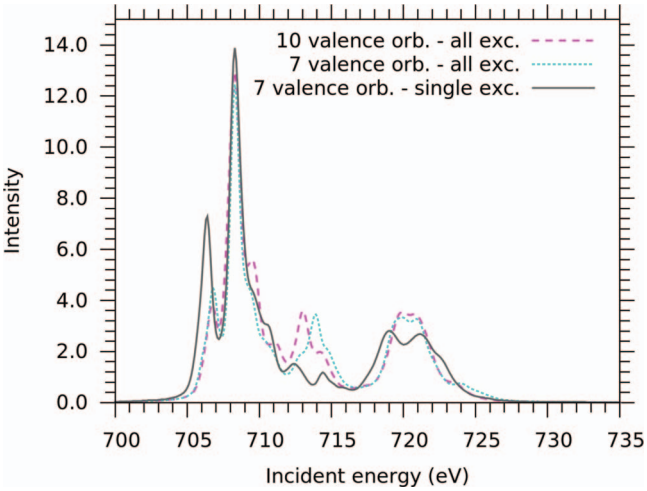

FIG. 8. L-edge XAS spectra of $[FeCl_6]^{3-}$ calculated with RASPT2-cc/ANO-RCC-VTZP, 80 states per symmetry and spin state, and different RAS spaces: (15,1,0:3,10,0) - 10 valence orbitals and all excitations, (15,1,0:3,7,0) - 7 valence orbitals and all excitations, and (15,1,3:3,5,2) - 7 valence orbitals and maximum 3 electrons in the e_g orbitals (single excitation).

710-715 eV region, with a blue shift of the ligand-to-metal shake-up transition by ∼1.0 eV. These results indicate that, for systems dominated by σ-bonding, active spaces with seven valence orbitals are sufficient to predict the L-edge spectra with good accuracy. Decreasing the active space by removing the filled ligand σ orbitals would further reduce computational cost, but this alternative could not be tested due to convergence problems in the RASPT2 calculations. The poor convergence is an indication of a strong correlation between e_g and σ orbitals and that these orbital pairs must be a part of the active space to get good results.

An alternative to reducing the number of active orbitals is to place some of the orbitals in the RAS3 space where the number of excitations can be limited. Putting the e_g orbitals in the RAS3 space and allowing a maximum of three electrons, (15,1,3;3,5,2), means that only one additional electron is allowed in the e_g orbitals from the $(t_{2g})^3(e_g)^2$ ground state configuration. Interestingly, the shake-up transition disappears, which confirms that this peak requires more than single-electron excitations to the e_g orbitals.

C. Ferricyanide ($[Fe(CN)_6]^{3-}$)

In $[Fe(CN)_6]^{3-}$, each cyanide ligand contributes one filled σ orbital and two empty antibonding orbitals of π type. Assuming O_h symmetry, two σ SALCs of e_g symmetry mix with metal 3d e_g orbitals to give ligand-dominated bonding (σ) and metal-dominated antibonding (e_g or σ^*) orbitals, see Fig. 1. Three empty CN π SALCs mix with Fe 3d t_{2g} orbitals to form metal-centered bonding (t_{2g} or π) and ligand-centered antibonding (π^*) orbitals that describe π backdonation.

In O_h symmetry, the ground state of ferricyanide is the low-spin $^2T_{2g}$ state with a nominal $(t_{2g})^5(e_g)^0$ electron configuration. The Jahn-Teller distortion due to the presence of five electrons in three t_{2g} orbitals leads to D_{4h} symmetry, but as the t_{2g} orbitals are weakly bonding the distortion is small. The effects on both the ground state energies and the final spectrum are also small, see Figs. 4 and 5 of the supplementary material.[54] Labels appropriate for O_h symmetry will therefore be used.

The RAS1 space again consists of the three Fe 2p (t_{1u}) orbitals. The RAS2 space has 10 orbitals. The empty metal-dominated e_g orbitals correlate with the two filled ligand σ, while the partially filled metal t_{2g} orbitals can either correlate with the ligand π^* orbitals or the metal 4d t'_{2g} orbitals. In the ground state, the t'_{2g} orbitals are better correlating partners and stay in the active space during the RASSCF optimization, see Fig. 6 of the supplementary material.[54] However, the state-average optimization with sufficient number of excited states to give direct π^* excitations leads to the solutions where the π^* orbitals are included in the active space instead of the t'_{2g} orbitals, see Fig. 6 of the supplementary material.[54]

The experimental L-edge XAS spectrum of ferricyanide, see Fig. 9, has three distinct features in the L_3 edge: a first peak at 705.8 eV assigned to a $2p \rightarrow t_{2g}$ transition, a second peak with a maximum around 710 eV, assigned to e_g transitions, and a third peak at around 712 eV assigned to π^* transitions.[51] The L-edge XAS spectrum calculated at the RASPT2-cc/ANO-RCC-VTZP 120 (15,1,0;3,10,0) level of theory captures all the major features of the experimental spectrum: the difference in intensity of the t_{2g} peaks in the two edges, the shape of the e_g resonance, the high intensity of the π^* resonance, as well as its high-energy shoulder, see Fig. 9. The main differences are the shift of the π^* peak to higher energy by ∼1.5 eV, and an underestimated splitting between the L_3 and L_2 edges by ∼1.0 eV. The accuracy of the core RAS spectrum is comparable to that achieved with the semi-empirical CTM model.

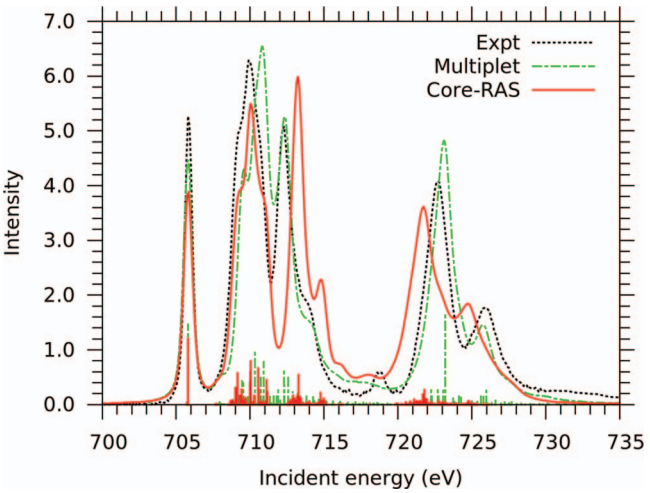

FIG. 9. L-edge XAS spectra of $[Fe(CN)_6]^{3-}$ from RASPT2-cc(15,1,0;3,10,0)/ANO-RCC-VTZP with 120 states (red solid line), from the semi-empirical charge-transfer multiplet model (green dashed-dotted line), and from experiment (black solid line).[51]

The molecular orbital contributions to the $[Fe(CN)_6]^{3-}$ L-edge XAS spectrum (cf. Fig. 10) can be analyzed in a similar way as previously done for Fe^{3+} and $[FeCl_6]^{3-}$. All resonances, except the first $2p \rightarrow t_{2g}$ transition, are comprised of excitations to a large number of multiplet states. For the broad $2p \rightarrow e_g$ resonance, the low-energy shoulder is a

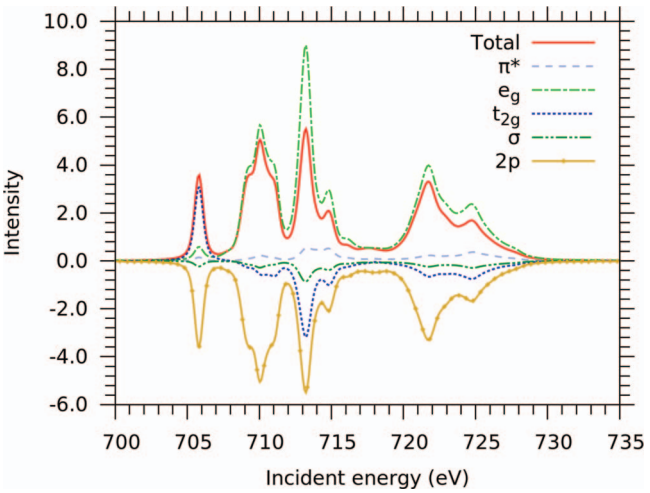

FIG. 10. Orbital analysis for the $[Fe(CN)_6]^{3-}$ L-edge XAS spectrum calculated with RASPT2-cc/ANO-RCC-VTZP (15,1,0;3,10,0) and 120 states per symmetry and spin state.

relatively pure e_g transition but with increasing energy the different $(t_{2g})^5(e_g)^1$ multiplets mix more strongly with other excited configurations. This appears as an increasing loss of electrons from the t_{2g} orbitals. The reason for the high intensity of the π^* peak, despite the small metal contributions to the π^* orbital, can also be rationalized. Here, the contributions from direct excitations into the π^* orbitals are relatively small, and instead an intensity borrowing from e_g excitations has a major effect.[51] There are also large changes in the occupation number of the t_{2g} orbitals, which reflects the increased weight of configurations with less than five t_{2g} electrons at this energy.

The calculations of ferric chloride showed that the number of orbitals in the RAS2 space could be decreased from ten to seven without significant changes to the spectrum. In ferricyanide, the three highest orbitals of t_{2g} symmetry are not included to describe correlation, but are ligand π^* orbitals required to describe the π^* peak. If these orbitals are removed, the π^* peak cannot be reproduced. This supports the assignment of this feature as a π^* backbonding peak.

To save computational time a few orbitals can instead be moved to the RAS3 space where the number of excitations can be limited. The spectra calculated with e_g and π^* orbitals placed in the RAS3 space, and allowing either two, RAS(15,1,2;3,5,5), or three, RAS(15,1,3;3,5,5), electrons are shown in Fig. 11. Since one of these electrons comes from the core excitation, these RAS calculations represent single and double excitations within the valence space, respectively. Allowing only two RAS3 electrons lead to significant changes in the spectrum and the π^* peak in the L_3-edge almost disappears. This is consistent with the orbital analysis above where the π^* peak had significant contributions from states with multiple excitations. Instead, allowing double excitations in the valence space, i.e., three RAS3 electrons, gives significantly better results. The main difference compared to the original calculation is a shift of the e_g peaks to higher energy.

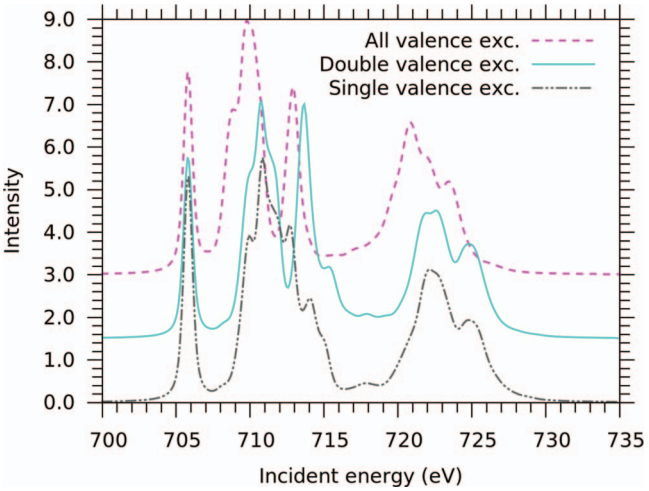

FIG. 11. L-edge XAS spectra of $[Fe(CN)_6]^{3-}$ calculated using RASPT2-cc/ANO-RCC-VTZP with 80 states and different number of excitations allowed in the e_g and π^* orbitals: (15,1,0:3,10,0) - all excitations, (15,1,3:3,5,5) - triple excitations, and (15,1,2;3,5,5) - double excitations.

IV. DISCUSSION

The results show that the core RAS method can predict L-edge XAS spectra at a level comparable to that of the semi-empirical CTM model. While the CTM model describes donation and backdonation through additional charge-transfer configurations, the core RAS model includes these effects by increasing the number of orbitals in the active space. An important difference is that adding configurations to the CTM model increases the number of model parameters, while the core RAS calculations are essentially parameter free, independent of the type of electronic structure to be described.

The two methods are most directly comparable for the Fe^{3+} ion that lack any charge-transfer parameters. However, there are still differences in the description of electron correlation and spin-orbit coupling. In the multiplet, model electron-electron repulsion is treated at the HF level, with a parameterized reduction of the integrals by 80%. The core RAS model improves on this description by calculating the 3d-3d and 2p-3d interactions through a full CI, while correlation with other electrons are included through second-order perturbation theory.

The core RAS method evaluates the spin-orbit coupling strengths on the correlated spin-free states through a perturbation approach, and subsequent diagonalization of the state interaction matrix gives SOC states, which are linear combinations of spin-free states. This approach, corresponding to molecular L-S coupling, is expected to work better for weak perturbations like 3d SOC than for the strong 2p SOC. The multiplet model improves on that description as it diagonalizes a state interaction matrix that includes both electron-electron repulsion and spin-orbit coupling. In the core RAS calculations, the low-energy $J' = \frac{1}{2}$ states in the L_2 edge mix strongly with high-energy $J' = \frac{3}{2}$ states of L_3 edge, which could be the reason for the larger deviations between these methods for energies above 715 eV, including the peak in the high-spin spectra that only appear in the core RAS calculations, see Figs. 3(a) and 3(b).

With performance comparable to that of the multiplet model, the core RAS approach is an attractive alternative for any small to medium-sized molecular system regardless of symmetry. It can be applied to systems with complicated electronic structures, e.g., orbitally degenerate ground states, and with proper design of the active space, effects of both ligand donor bonding and back-donation can be described. As all possible excitations are included, the method also reproduces spectral features arising from multiple excitations, e.g., shake-up and shake-down transitions.

A major drawback of the core RAS method is the relatively high computational cost. Although this method gives better results for $[FeCl_6]^{3-}$ than the DFT/ROCIS method, the latter can be applied to much larger systems. The core RAS method is thus best suited for the simulation of spectra dominated by local effects. The current calculations have been performed on relatively small metal clusters without taking counter ions or adjacent metal ions into account. The core RAS results can possibly be improved by including a better description of the environmental effects. However, the good agreement with experimental spectra reveals that the effects

beyond the first coordination shell are relatively small for the current systems.

One of the appealing features of the core RAS approach is the possibility to analyze the L-edge XAS spectrum in terms of contributions from chemically intuitive molecular orbitals. A new scheme was therefore developed that takes into account the changes in natural occupation number of the orbitals during the core excitation. This analysis shows the importance of the correlation between metal and ligand orbitals and can also be used to identify the origin of an peak, as shown by the $[FeCl_6]^{3-}$ shake-up transition. However, this analysis does not take into account changes in the shape of the orbitals during the RASSCF optimization, e.g., when the $[FeCl_6]^{3-}$ metal-centered t'_{2g} orbitals are replaced by Cl 4p orbitals. Fortunately, orbital rotation mainly occurs for weakly correlating orbitals that have small changes in occupation number. Furthermore, many of the metal-ligand bonds in RASSCF calculations have excessively ionic nature. The subsequent RASPT2 step only corrects the energies but does not change the reference orbitals. Care must therefore be taken when extracting quantitative metal-ligand covalencies directly from the RASSCF calculations.

Although core RAS is essentially an *ab initio* method, it is important to realize that the results are sensitive to some model selections, in particular the active space. This does not make it less *ab initio*, as the most optimal calculation is always the one using the largest active space. However, as large active spaces cannot always be afforded, different approaches to reduce the computational time can lead to different final results. It is therefore important to properly understand the effects on the spectra.

Systematic investigations on transition metal complexes show that large active spaces are required to calculate accurate relative energies of different states.[58] One important consideration is the double-shell effect.[32] In $[FeCl_6]^{3-}$, inclusion of a set of empty t'_{2g} orbitals only has a minor effect on the calculated spectrum, see Fig. 8. The main reason is the relatively low accuracy required in calculations of L-edge XAS spectra, since they span an energy region of more than 30 eV.

The use of a RAS3 space for the valence orbitals gives considerable flexibility in the quality of the CI calculation and can lead to significant savings in computational time. Allowing a single excitation into the RAS3 space captures the main 2p excitation, while excitation of a additional valence electrons enables the description of shake-up (and shake-down) transitions, as shown for $[FeCl_6]^{3-}$ in Fig. 8. In RAS calculations, excitations are also used to describe electron correlation, which requires at least double-excitations in the valence space. Thus for $[Fe(CN)_6]^{3-}$, allowing three excitations, including the core excitation, gives a spectrum similar to the full CI while the calculation with only two excitations did not, see Fig. 11. In the latter case, the RASPT2 step does not help because it adds correlation between different orbital spaces but does not recover missing correlation within the active space.

The spectral simulations in this study have been performed with the 2p orbitals in the RAS1 space allowing maximum one hole. This is the preferred approach for centrosymmetric systems, since all valence excitations keep "gerade" symmetry and only 2p excitations lead to states with "ungerade" symmetry. In absence of inversion symmetry, a large number of unwanted valence excited states will have lower energy than the core hole excited states. Another possibility is then to put the 2p orbitals in the RAS3 space and allowing a maximum of 5 electrons. A drawback of the core RAS3 approach, compared to the core RAS1 approach, is that 3-4 times more determinants have to be calculated. Moreover, the RAS3 space can no longer be used to tune the number of valence excitations.

In the current procedure, the 2p orbitals are excluded from the RASSCF orbital optimization. The effect of neglecting core relaxation has not been evaluated but as the sudden approximation performs well for many X-ray processes, such a relaxation is believed to be relatively small, at least for the relative energies of different final states.

As the core RAS method describes all final states reached through core excitations, it can potentially be applied to a various X-ray experiments. The direct connection between the X-ray spectrum and a molecular orbital picture makes it attractive for analyzing the electronic structures of different compounds and the method can be used to extract the electronic structure of a complex without any prior assumptions. One potential application of the core RAS method is for heme systems, primarily studied using the intense porphyrin $\pi \rightarrow \pi^*$ transitions in the UV/Vis region. For these systems insights into the electronic structure of the iron are complicated due to the intense ligand features that obscure the Fe center. Another possibility is to analyze the electronic structure of transition-metal catalysts in photoactivated systems, where the chromophores obscure many UV/Vis probes of the catalyst itself. The explicit calculation of the excited states also makes it possible to follow the nuclear dynamics of core excited states reached in ultra-fast X-ray experiments.

V. CONCLUSIONS

Multiconfigurational wavefunction (RASSCF/ RASPT2) theory has great potential for simulations of X-ray processes as it includes a high-level description of electron-electron correlation together with a perturbation treatment of spin-orbit coupling. The core RAS method can be applied to any medium-sized system without any formal symmetry constraints. Among the advantages is that it handles orbitally degenerate ground states, describes metal-ligand charge transfer, and includes all possible electron excitations, at least within the active orbitals. In calculations of L-edge XAS spectra of a series of ferric systems, the performance of the core RAS method is comparable to that of the commonly used semi-empirical CTM multiplet model. This is achieved without the use of any system-dependent parameters.

The flexibility of the method makes it possible to tune the balance between accuracy and computational cost. Compared to valence excitations, the size of the valence active space can be reduced as the required accuracy is typically much lower. The number of valence excitations can be limited through the use of a RAS3 space, although to achieve results comparable to a full CI in the active space, it is recommended to allow at least two valence excitations in addition to the core excitation.

The high accuracy of the core RAS results make them useful in fingerprinting the electronic structures of molecular systems without any prior knowledge. The analysis of the X-ray spectra in terms of molecular orbital contributions enables a direct connection between a spectrum and the electronic structure features. The core RAS method can therefore be of great use in the interpretation of a wide variety of different X-ray experiments.

ACKNOWLEDGMENTS

Financial support was provided by the Carl Trygger Foundation (R.V.P. and M.O.), the Marcus and Amalia Wallenberg Foundation (M.L.), and the Swedish Research Council (M.O. and M.L.). The computations were performed on resources provided by SNIC through Uppsala Multidisciplinary Center for Advanced Computational Science (UPPMAX) under project s00112-267 and National Supercomputer Centre at Linköping University under project liu-2012-00060-46.

[1]R. Laskowski and P. Blaha, Phys. Rev. B **82**, 205104 (2010).
[2]J. Vinson, J. Rehr, J. Kas, and E. Shirley, Phys. Rev. B **83**, 115106 (2011).
[3]P. Krüger and C. R. Natoli, Phys. Rev. B **70**, 245120 (2004).
[4]P. Krüger, Phys. Rev. B **81**, 125121 (2010).
[5]F. De Groot, J. Fuggle, B. Thole, and G. Sawatzky, Phys. Rev. B **42**, 5459 (1990).
[6]A. Tanaka and T. Jo, J. Phys. Soc. Jpn. **63**, 2788 (1994).
[7]F. d. Groot, Coord. Chem. Rev. **249**, 31 (2005).
[8]K. Ogasawara, T. Iwata, Y. Koyama, T. Ishii, I. Tanaka, and H. Adachi, Phys. Rev. B **64**, 115413 (2001).
[9]H. Ikeno, T. Mizoguchi, Y. Koyama, Y. Kumagai, and I. Tanaka, Ultramicroscopy **106**, 970 (2006).
[10]M. W. Haverkort, M. Zwierzycki, and O. K. Andersen, Phys. Rev. B **85**, 165113 (2012).
[11]M. Roemelt, D. Maganas, S. DeBeer, and F. Neese, J. Chem. Phys. **138**, 204101 (2013).
[12]D. Maganas, M. Roemelt, T. Weyhermüller, R. Blume, M. Hävecker, A. Knop-Gericke, S. DeBeer, R. Schlögl, and F. Neese, Phys. Chem. Chem. Phys. **16**, 264 (2014).
[13]E. Otero, N. Kosugi, and S. G. Urquhart, J. Chem. Phys. **131**, 114313 (2009).
[14]I. Josefsson, K. Kunnus, S. Schreck, A. Fhlisch, F. de Groot, P. Wernet, and M. Odelius, J. Phys. Chem. Lett. **3**, 3565 (2012).
[15]H. Ikeno, I. Tanaka, Y. Koyama, T. Mizoguchi, and K. Ogasawara, Phys. Rev. B **72**, 075123 (2005).
[16]H. Ikeno, T. Mizoguchi, and I. Tanaka, Phys. Rev. B **83**, 155107 (2011).
[17]G. Capano, T. Penfold, N. Besley, C. Milne, M. Reinhard, H. Rittmann-Frank, P. Glatzel, R. Abela, U. Rothlisberger, M. Chergui *et al.*, Chem. Phys. Lett. **580**, 179 (2013).
[18]B. O. Roos, "The complete active space self-consistent field method and its applications in electronic structure calculations," in *Advances in Chemical Physics* (John Wiley & Sons, Inc., 2007), pp. 399–445.
[19]J. Olsen, B. O. Roos, P. Jørgensen, and H. J. A. Jensen, J. Chem. Phys. **89**, 2185 (1988).
[20]P.-Å. Malmqvist, A. Rendell, and B. O. Roos, J. Phys. Chem. **94**, 5477 (1990).
[21]K. Andersson, P.-Å. Malmqvist, B. O. Roos, A. J. Sadlej, and K. Wolinski, J. Phys. Chem. **94**, 5483 (1990).
[22]K. Andersson, P.-Å. Malmqvist, and B. O. Roos, J. Chem. Phys. **96**, 1218 (1992).
[23]P.-Å. Malmqvist, K. Pierloot, A. R. M. Shahi, C. J. Cramer, and L. Gagliardi, J. Chem. Phys. **128**, 204109 (2008).
[24]R. Klooster, R. Broer, and M. Filatov, Chem. Phys. **395**, 122 (2012).
[25]I. Josefsson, S. K. Eriksson, N. Ottosson, G. Ohrwall, H. Siegbahn, A. Hagfeldt, H. Rensmo, O. Bjorneholm, and M. Odelius, Phys. Chem. Chem. Phys. **15**, 20189 (2013).
[26]P. Wernet, K. Kunnus, S. Schreck, W. Quevedo, R. Kurian, S. Techert, F. M. de Groot, M. Odelius, and A. Fohlisch, J. Phys. Chem. Lett. **3**, 3448 (2012).
[27]S. I. Bokarev, M. Dantz, E. Suljoti, O. Kühn, and E. F. Aziz, Phys. Rev. Lett. **111**, 083002 (2013).
[28]K. Atak, S. I. Bokarev, M. Gotz, R. Golnak, K. M. Lange, N. Engel, M. Dantz, E. Suljoti, O. Kühn, and E. F. Aziz, J. Phys. Chem. B **117**, 12613 (2013).
[29]N. Engel, S. I. Bokarev, E. Suljoti, R. Garcia-Diez, K. M. Lange, K. Atak, R. Golnak, A. Kothe, M. Dantz, O. Kühn, and E. F. Aziz, J. Phys. Chem. B **118**, 1555 (2014).
[30]K. Kunnus, I. Josefsson, S. Schreck, W. Quevedo, P. S. Miedema, S. Techert, F. M. F. de Groot, M. Odelius, P. Wernet, and A. Fhlisch, J. Phys. Chem. B **117**, 16512 (2013).
[31]F. Aquilante, L. De Vico, N. Ferré, G. Ghigo, P.-Å. Malmqvist, P. Neogrády, T. B. Pedersen, M. Pitoňák, M. Reiher, B. O. Roos, L. Serrano-Andrés, M. Urban, V. Veryazov, and R. Lindh, J. Comput. Chem. **31**, 224 (2010).
[32]K. Pierloot, Mol. Phys. **101**, 2083 (2003).
[33]J. Finley, P.-Å. Malmqvist, B. O. Roos, and L. Serrano-Andrés, Chem. Phys. Lett. **288**, 299 (1998).
[34]G. Ghigo, B. O. Roos, and P.-Å. Malmqvist, Chem. Phys. Lett. **396**, 142 (2004).
[35]N. Forsberg and P.-Å. Malmqvist, Chem. Phys. Lett. **274**, 196 (1997).
[36]M. Douglas and N. M. Kroll, Ann. Phys. (N.Y.) **82**, 89 (1974).
[37]B. A. Hess, Phys. Rev. A **33**, 3742 (1986).
[38]B. O. Roos, R. Lindh, P.-Å. Malmqvist, V. Veryazov, and P.-O. Widmark, J. Phys. Chem. A **109**, 6575 (2005).
[39]B. O. Roos, R. Lindh, P.-Å. Malmqvist, V. Veryazov, and P.-O. Widmark, J. Phys. Chem. A **108**, 2851 (2004).
[40]F. Aquilante, T. B. Pedersen, and R. Lindh, J. Chem. Phys. **126**, 194106 (2007).
[41]F. Aquilante, P.-Å. Malmqvist, T. B. Pedersen, A. Ghosh, and B. O. Roos, J. Chem. Theory Comput. **4**, 694 (2008).
[42]J. Boström, M. G. Delcey, F. Aquilante, L. Serrano-Andrés, T. B. Pedersen, and R. Lindh, J. Chem. Theory Comput. **6**, 747 (2010).
[43]B. A. Hess, C. M. Marian, U. Wahlgren, and O. Gropen, Chem. Phys. Lett. **251**, 365 (1996).
[44]B. O. Roos and P.-Å. Malmqvist, Phys. Chem. Chem. Phys. **6**, 2919 (2004).
[45]P.-Å. Malmqvist and B. O. Roos, Chem. Phys. Lett. **155**, 189 (1989).
[46]P.-Å. Malmqvist, B. O. Roos, and B. Schimmelpfennig, Chem. Phys. Lett. **357**, 230 (2002).
[47]J. K. Beattie and C. J. Moore, Inorg. Chem. **21**, 1292 (1982).
[48]J. W. Lauher and J. A. Ibers, Inorg. Chem. **14**, 348 (1975).
[49]M. Kovsarnechan, J. Roziere, and D. Mascherpa-Corral, J. Inorg. Nucl. Chem. **40**, 2009 (1978).
[50]J. C. A. Boeyens, A. Forbes, R. D. Hancock, and K. Wieghardt, Inorg. Chem. **24**, 2926 (1985).
[51]R. K. Hocking, E. C. Wasinger, F. M. F. de Groot, K. O. Hodgson, B. Hedman, and E. I. Solomon, J. Am. Chem. Soc. **128**, 10442 (2006).
[52]E. Stavitski and F. M. de Groot, Micron **41**, 687 (2010).
[53]E. C. Wasinger, F. M. F. de Groot, B. Hedman, K. O. Hodgson, and E. I. Solomon, J. Am. Chem. Soc. **125**, 12894 (2003).
[54]See supplementary material at http://dx.doi.org/10.1063/1.4896373 for multiplet parameters, shift of energies of the L-edge spectrum, schematics of SOC energy levels, molecular orbitals, and various core-RAS calculated L-edge spectra of ferricyanide and ferric chloride.
[55]M. O. Krause and J. H. Oliver, J. Phys. Chem. Ref. Data **8**, 329 (1979).
[56]M. Ohno and G. A. van Riessen, J. Electron Spectrosc. **128**, 1 (2003).
[57]M. Lundberg, T. Kroll, S. DeBeer, U. Bergmann, S. A. Wilson, P. Glatzel, D. Nordlund, B. Hedman, K. O. Hodgson, and E. I. Solomon, J. Am. Chem. Soc. **135**, 17121 (2013).
[58]S. Vancoillie, H. Zhao, V. T. Tran, M. F. Hendrickx, and K. Pierloot, J. Chem. Theory Comput. **7**, 3961 (2011).